TOPICAL REVIEW

Dynamics of polynucleotide transport through nanometre-scale pores

Amit Meller

The Rowland Institute at Harvard, Harvard University, Cambridge, MA 02142, USA

E-mail: meller@rowland.harvard.edu

Abstract
The transport of biopolymers through large membrane channels is a ubiquitous
process in biology. It is central to processes such as gene transfer by
transduction and RNA transport through nuclear pore complexes. The transport
of polymers through nanoscopic channels is also of interest to physicists
and chemists studying the effects of steric, hydrodynamic, and electrostatic
interactions between polymers and confining walls. Single-channel ion current
measurements have been recently used to study the transport of biopolymers,
and in particular single-stranded DNA and RNA molecules, through nanometre-
size channels. Under the influence of an electric field, the negatively charged
polynucleotides can be captured and drawn through the channel in a process
termed 'translocation'. During translocation, the ion current flowing through
the channel is mostly blocked, indicating the presence of the polymer inside
the channel. The current blockades were found to be sensitive to the properties
of the biopolymers such as their nucleotide composition, length, and secondary
structure, and to physical parameters such as the driving field intensity,
temperature, and ionic strength. These blockades are therefore a rich source
of information regarding the dynamics of polynucleotides in the pore. The
translocation process is separated into its two main steps: (a) polymer 'capture'
in which one of the polymer's ends is threaded a small distance through the
channel, and (b) polymer sliding through the channel. The experimental and
theoretical efforts to elucidate polymer capture and the transport dynamics of
biopolymers in nanoscopic pores are reviewed in this article.

Contents

1. Introduction

Large membrane channels were designed by Nature to regulate the transport of biomolecules such as proteins and nucleic acids, and to serve as pathways to metabolites [1]. The size of these channels is on the nanometre scale, roughly from 1 to ∼50 nm, and unlike channels of excitable membranes that exhibit high ion selectivity, large channels have poor ion selectivity [2]. Examples of large channels include bacterial porins, mitochondrial channels, some toxin channels, the nuclear pore complex, and protein conducting channels in the endoplasmic reticulum [3]. Many processes in biology involve the transport of biopolymers across large channels embedded in the plasma or the cell-nucleus membranes [4]. Examples include gene transfer by transduction [5, 6], gene swapping through bacterial pili [7, 8], RNA and transcription factor transport through nuclear pore complexes [9–12], and the uptake of oligonucleotides by some membrane proteins [13]. Despite the wide interest in these processes, the physical rules governing the dynamics of the biopolymers inside these channels is to date largely unknown, and the study of polymer dynamics remains an important and fascinating field.

In addition to its biological relevance, the transport dynamics of polymers through nanometre-size pores ('nanopores') is of fundamental interest for physicists and chemists. Because the diameter of these channels is not much larger than the polymers passing through them, the transport dynamics in these small constrictions is a result of multiple factors including steric, hydrodynamic, and electrostatic interactions [3]. Elucidation of the transport dynamics of biopolymers in nanopores is highly relevant to the growing field of microfluidics and in particular to recent efforts to miniaturize molecular biology reactions to the sub-micron scale [14]. The passage of polymers through nanopores can be seen as a one-dimensional version of polymer 'trapping' in random environments such as gels or reptation in porous media [15]. Unlike gel systems, a nanopore involves a *single* confining volume (gels typically involve many polydisperse pores); therefore the theoretical analysis of the polymer dynamics in the pore is greatly simplified and computer simulations are made more accessible.

The transport of nucleic acids and other analytes through nanopores, and in particular through the alpha-toxin channel (α-HL) protein pore, constitutes the basis for numerous technological applications in the past few years:

 (I) It was shown that by drawing single-stranded DNA or RNA molecules through the pore, information regarding their structure, base composition, and dynamic properties could be obtained [16–20].

 (II) The stability of hairpin DNA molecules was probed by temporarily lodging a DNA duplex in the internal cavity of the pore (the 'vestibule'; see below), allowing the rapid discrimination between different types of DNA hairpin molecule [21].

(III) A sensor based on DNA hybridization between a short single-stranded DNA fragment covalently anchored to the α-HL pore and a matching oligonucleotide was demonstrated [22].

(IV) Genetically modified α-HL pores were engineered to include a single divalent metal cation binding site. The binding of metal ions reduced the ionic current flowing through the pore, thus indicating the binding kinetics [23, 24].

Organic analytes could also be detected using a similar concept by equipping the wild-type channel with an internal, non-covalently bound molecular adapter which mediated channel blocking by the analyte[1] [25].

This review focuses on a single aspect in the field: the transport dynamics of a polymer drawn inside a nanoscopic channel. Primarily, the dynamics of polynucleotides (DNA or RNA) is discussed, leaving the reviewing of uncharged polymers (such as polyethylene glycol) to other papers. However, some of the concepts that are discussed in this review apply to uncharged polymers. Also, the practical applications of the pore as a biosensor or chemical probe [26] is not discussed here.

The organization of this article is as follows. In section 2 the concepts underlying nanopore experiments are reviewed, starting with their historical roots, the 'Coulter counter' method. Because most of the results presented in this article make use of the α-toxin pore, a short description of the pore structure is given. In section 3, the theoretical models describing the polymer dynamics inside the pore and the total polymer flux through the pore are discussed. Our aim is to give the reader an idea of the relevant physics of these models, and not to present detailed derivations that can be found in the references cited. In section 4, a review of the experimental results is provided. This section is divided into two subsections: the first deals with the transport of the polymers from the bulk to the pore (until one of the polymers' ends is captured), and the second is devoted to the polymer dynamics inside the channel. Section 5 is a summary and discussion of future directions in the field.

2. The nanopore detection concept

The concept underlying nanopore detection is based on the resistive method for particle counting and sizing in conducting fluid, which was invented by Coulter in the early 1950s [27] and later refined by DeBlois and Bean [28]. In the Coulter counter small particles were forced by pressure difference through a small aperture (on the micrometre scale) made in an insulating wall such as glass. When the particles passed through the aperture they displaced the electrolyte in the solution, causing blockades in an ionic current flowing through the aperture, observed as momentary change in the conductance of the aperture (see figure 1). The magnitude of these blockades was roughly proportional to the volume of each particle, and depended somewhat on the particle shapes.

With the aid of modern current amplifier instrumentation the 'Coulter counter' approach was extended to the molecular scale [3]. In a simple but very informative experiment, Bezrukov and co-workers [29] demonstrated that the magnitude of the ion current flowing through a single

---

[1] The concept of stochastic sensing using pores was recently described by Bayley and Cremer [26].
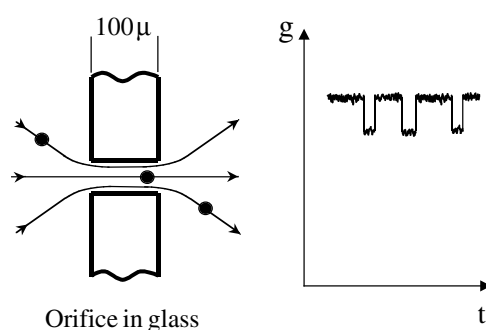
Figure 1. The Coulter counter concept: a flow of liquid through a small orifice made in a thin wall is maintained by a pressure difference. The flow can carry micrometre-sized particles that produce pulses in the capillary conductance, g. The number of pulses s^{-1} indicates the particle concentration; the particle size can be inferred from the pulse amplitude. This drawing was adapted from [3] with permission.

20 Å alamethicin channel was reduced and became noisier upon the addition of poly(ethylene glycol) to the system. Analysis of the current fluctuations made it possible to estimate the diffusion coefficient of the polymers inside the channel. Kasianowicz and co-workers [16] showed that an electric field can drive single-stranded DNA (ssDNA) and RNA polynucleotides through the water-filled α-HL channel and that the passage of each polynucleotide is signalled by the blockade in the channel current. The quantitative polymerase chain reaction (PCR) of the molecules in the '*trans*' chamber (see figure 2) after such an experiment confirmed that the DNA did indeed translocate from one side of the membrane to the other side. In parallel, Szabò *et al* [30] conducted experiments with reconstituted *Bacillus subtilis* ion channels, demonstrating that double-stranded DNA can translocate through these pores under the influence of osmotic pressure and/or electrical field.

In a typical translocation experiment, a single protein pore (α-HL described below) is self-assembled in a phospholipid bilayer membrane formed over a small aperture. The aperture (20–100 μm) is made in a thin Teflon film or, alternatively, fabricated at the end of a small
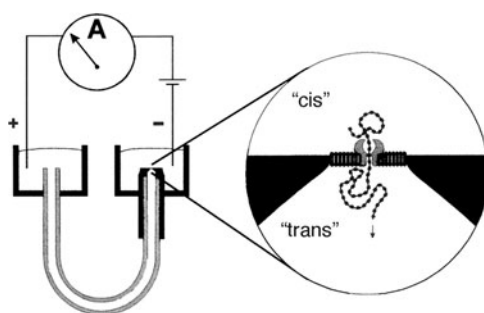

Figure 2. A horizontal bilayer apparatus made by fabricating a $\sim$25 μm aperture on one end of a small Teflon tube. The U-shaped tube connects two 70 μl chambers milled into a Teflon support (left). The chambers and the tube are filled with salt buffer and are connected to a patch-clamp head-stage by two Ag–AgCl electrodes. A phospholipid bilayer is formed across the 25 μm aperture (right, not to scale), and a single α-haemolysin channel is reconstituted into the membrane. Nucleic acids are driven through the channel by applied voltage across the insulating membrane, with the positive pole connected to the *trans* side. The two chambers can be embedded in a temperature-regulated copper block [18]. This picture was adapted from [17] with permission.
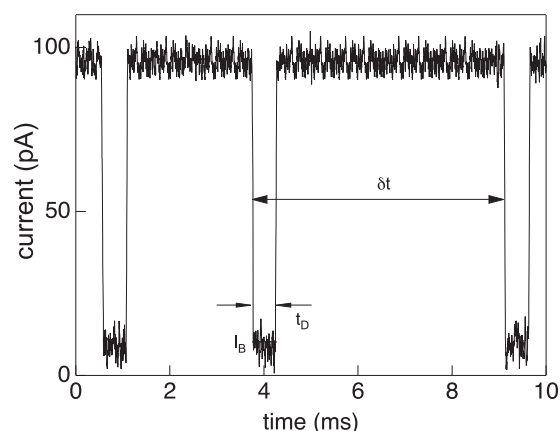
Figure 3. Translocation events. When the DNA polynucleotides enter the pore, the current drops from its initial value of ~100 pA to a blocked level of ~10 pA ($V = 120$ mV, $T = 15\,°C$). The blocked current level is observed during translocation of the polymer through the channel, and the current is restored to its original value when the DNA exits from the other side of the membrane. Three successive translocation events are displayed. We denote the translocation duration of each event as t_D, the elapsed time between successive events δt, and the average blocked current value, I_B. The data were acquired with a 100 kHz low-pass filter, digitized and analysed at 333 kHz/12 bits. For the display the data were digitally filtered at 10 kHz. This figure was adapted from [32].

'U'-shape Teflon tube (figure 2). The plastic film and the membrane separate two fluid chambers filled with high-ionic-strength buffer (typically 1 M KCl), that are in contact with a pair of electrodes, which convert Cl^- ions in the fluid to electrons in the leads. Phospholipid membranes form a low-leakage contact with Teflon yielding a ~10^{11} Ω seal and relatively low noise. The excellent seal, the low dielectric constant of the membrane, and the low resistance of the buffer permit high-bandwidth measurements of the electric current (typically on the ~pA scale and up to ~100 kHz). With the 'U' tube configuration of the experimental apparatus [17] it is possible to reduce the buffer chamber volumes to below 100 μl, and to regulate the temperature of the system precisely [18].

The flowing ionic current level through the α-HL pore is very stable and depends on external parameters such as the ionic strength, temperature, and applied voltage in a predictable way. The pore exhibits 'gating' behaviour in acidic conditions, but stays open and stable over extended times above a pH of ~7.5 [31]. In particular, the open pore current was found to be stable over a period of days in experiments performed at pH 8.5 and in a temperature range of 2–22 °C [32]. Single-stranded DNA (ssDNA) or RNA molecules can be added to the '*cis*' or the '*trans*' side of the membrane. In the first case, applying a positive potential at the '*trans*' electrode causes the negatively charged polymers to enter the pore and slide through the channel from one side of the membrane to the other. This process is driven by the electric field gradient across the membrane, and hence it is commonly referred to as 'driven translocation'. During translocation the pore current is mostly blocked: upon the entry of the polymer to the α-HL channel the open pore current is abruptly decreased to ~10% of its original value. This transition is sharp and can be readily detected. A current trace acquired over 10 ms of experiment time (at 15 °C) is displayed in figure 3. Three blockade events corresponding to three ssDNA molecules (poly(dA)$_{100}$) are detected. The translocation duration, t_D, the time between successive events, δt, and the averaged blockade current, I_B, are measured for each event. These three quantities and their distributions are the basic information extracted
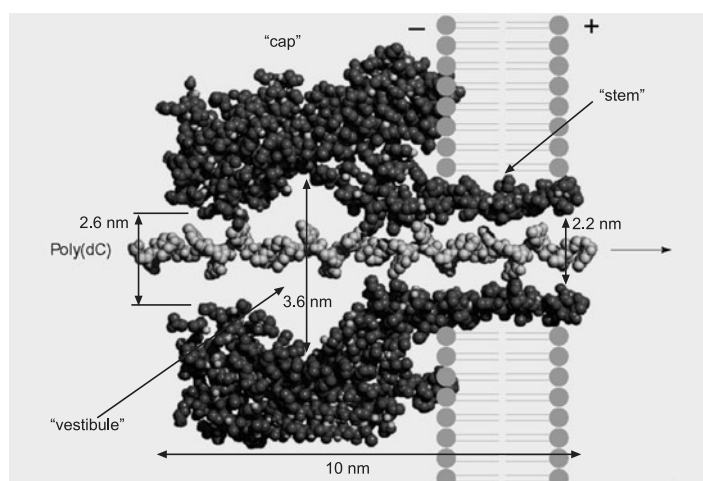
Figure 4. A single α-haemolysin channel is shown in cross-section embedded in a lipid bilayer. Also depicted is a translocating ssDNA molecule. The stem of the complex spans the lipid bilayer, and the cap part resides on the '*cis*' side. The pore dimensions noted in the figure are based on the protein coordinates of the crystal structure determined by Song *et al* [39]. The 1.5 nm limiting aperture at the entrance to the channel is composed of alternating glutamate and lysine residues. A voltage applied across the membrane can drive a single strand of poly(dC) through the pore as shown in the figure. This figure was modified from [61] with permission from the authors.

from the translocation experiments. As discussed in section 4, δt is mostly sensitive to bulk concentration [32, 33], whereas t_D and I_B are sensitive to the polynucleotide characteristics (length, sequence, secondary structure, ssDNA versus RNA, etc) [17, 18]. All the parameters depend strongly on the electric field.

Alpha haemolysin (or α-toxin) is secreted by *Staphylococcus aureus* as a water-soluble single-chain polypeptide with a mass of 33.2 kDa [34]. Membrane bound monomers assemble to form a 232.4 kDa heptameric transmembrane channel [35]. This protein complex is believed to induce apoptosis (cell death) in different cell types including rabbit erythrocytes, human erythrocytes, monocytes, and lymphocytes [34, 36], by two separate mechanisms: K^+ efflux and Na^+ influx through the plasma membrane and insertion in the outer mitochondrial membrane that results in triggering of cytochrome c release [37]. An effective diameter of 11.4 ± 0.4 Å has been estimated from the conductance of single oligomers [38]. More recently, the structure of the α-HL has been determined at 1.9 Å resolution, revealing a mushroom-shaped homo-oligomeric heptamer that contains a solvent-filled channel, 100 Å in length and 14–46 Å in diameter [39] (see figure 4). The 'cross-sectional' view of the pore complex can be separated into two parts: a roughly 100 Å in diameter extramembranal part ('cap'), and a transmembrane β-barrel channel ('stem'). The internal cavity in the cap (the 'vestibule') part upholds a 26 Å entrance and has a maximum diameter of $\sim$36 Å. The β-barrel channel is believed to be hydrophilic with a 15 Å limiting aperture at its entrance. The internal volume of the pore is $\sim$18 nm^3. On average, $\sim$600 H$_2$O molecules can be accommodated in the stem part, and at 1 M KCl conditions, $\sim$11 K$^+$ and $\sim$11 Cl$^-$ molecules reside in the channel [20].

3. Theoretical treatments of polymer dynamics inside pores

Several theoretical models have been developed to account for the DNA (and RNA) dynamics in the nanopore. Here some of these approaches are briefly reviewed and their compatibility with

the translocation experiments is examined. The theoretical section is organized as follows. First a coarse-grained description of forced translocation is presented. Second, we present models that involve the crossing of a free energy barrier arising due to the polymer's restricted configurations. Third, Monte Carlo simulations of more realistic polymers are presented. Fourth, the dynamics of polymer entry into the pore and the total polymer flux (i.e. the number of translocation events per unit time) are discussed. Finally a model that considers a specific interaction potential between the polymer and the pore is presented.

3.1. Coarse description of polymer translocation

Before considering the parts of the polymer outside the channel, it is useful to write down a coarse, translationally invariant (under integer multiples of the polymer unit length a in each direction) description of the problem, that captures some of the fundamental physical parameters of forced polymer translocation. Following the analysis given by Lubensky and Nelson [40] we introduce the probability $P(x, t)$ that a contour length x of the polymer's backbone has passed through the pore at time t (see also [40]). The polymer has a length L, and $x = 0$ when the polymer enters the pore. The probability current density of the polymer, $j(x, t)$ is defined by the continuity equation $\partial P/\partial t + \partial j/\partial x = 0$. For a single polymer, j is assumed to be linear in P, without higher-order terms:

$$j(x, t) = vP(x, t) - D\frac{\partial P(x, t)}{\partial x}.$$ (1)

The probability $P(x, t)$ then satisfies a diffusion equation with drift (due to the electric field):

$$\frac{\partial P}{\partial t} = D\frac{\partial^2 P}{\partial x^2} - v\frac{\partial P}{\partial x}$$ (2)

where D and v are respectively an effective diffusion coefficient and an average drift velocity. On the macroscopic level of this equation, all the information on the competition between the driving forces and the thermal spreading is encoded in a single parameter, $l_d \equiv D/v$, termed the diffusive length [40]. On length scales shorter than l_d the polymer's motion is governed by thermal forces, whereas on length scales longer than l_d the electric field dominates.

The crude analysis presented above can be directly related to the measured translocation time: the distribution of passage times can be obtained by solving equation (2) on the interval $[0, L]$ with absorbing boundary conditions $P(0) = P(L) = 0$, yielding a single-peaked function. We denote the peak value as t_P and the width of the distribution as δt_P. The ratio $\delta t_P/t_P$ can be expressed in terms of l_d/L and v [40]. By comparison of $\delta t_P/t_P$ with the experimental data, an estimate of l_d/L can be obtained. A typical experimental value for $\delta t_P/t_P$ is ~0.5 for polynucleotides 200 bases in length [16], which corresponds to a value of $l_d/L \approx 0.2$ or $l_d \sim 40a$ [40].

The parameters defined above provide an idea of the factors involved in the translocation process. In particular, it is possible to obtain an upper limit estimation of the effective diffusion coefficient in the pore, $D = l_d v$, by setting $l_d \approx L$ and v to the average drift velocity obtained in the experiments. Plugging in $L \approx 5$ nm (for $N = 12$) and $v \sim 10^{-2}$ cm s^{-1} (measured at 120 mV and room temperature) we obtain $D \sim Lv \sim 5 \times 10^{-9}$ cm^2 s^{-1} [19]. We note that this value is roughly *two orders of magnitude smaller* than the effective bulk diffusion for ssDNA having the same length [41]. The polymers' dynamics in the pore is thus highly impeded, as one would expect.
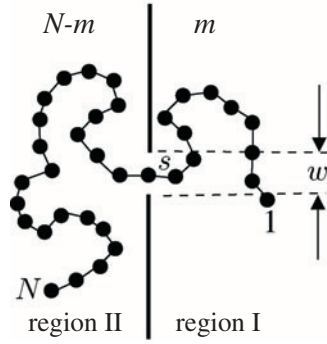
Figure 5. A schematic representation of a polymer with N units in the process of translocation through a hole of size w in a two-dimensional wall. The translocation coordinate s is the number of monomers on the exit ('*trans*') side. This figure was modified from [48] with permission.

3.2. Calculations of polymer translocation time in the presence of a free energy barrier

The problem of polymer translocation through a pore in a membrane was modelled by Sung and Park [42], and later by Muthukumar [43, 44] by considering a two-dimensional space divided by a thin wall. At the centre of the wall is a small hole that is wide enough for the polymer to thread through to the other side (see figure 5). The space is split into regions I and II: region I contains m monomers of the polymer and region II contains $N - m$ monomers, where N represents the total number of monomers in the chain. The partition function for a polymer chain of m segments in a semi-infinite space bounded by a hard wall when one end of the polymer is anchored to the wall is given by [45]

$$z_m \sim m^{\gamma - 1} \tag{3}$$

where $\gamma = 0.5$, ≈ 0.69, and 1 for Gaussian, self-avoiding, and rod-like chains respectively. The free energy associated with this polymer configuration is

$$\beta F_m = (1 - \gamma) \ln(m) + (1 - \gamma) \ln(N - m) + m\beta \, \Delta\mu, \tag{4}$$

where constant terms are ignored. $\beta = \frac{1}{k_B T}$, with k_B the Boltzmann constant and T the absolute temperature. For simplicity, γ is assumed to be identical on either side of the wall (a more general solution is described elsewhere) [43], and $\Delta\mu = \mu_2 - \mu_1$ is the chemical potential difference between the two sides. Equation (4) describes the free energy barrier reflecting the loss of polymer degrees of freedom when it is partitioned by the wall. The energy term ($m\beta \, \Delta\mu$) introduces a linear shift in the barrier's baseline.

The transport of the polymer across the nanopore can be described by a master equation [43]:

$$\frac{\partial P_m(t)}{\partial t} = u_{m-1} P_{m-1}(t) + w_{m+1} P_{m+1}(t) - (u_m + w_m) P_m(t), \tag{5}$$

where $P_m(t)$ is the probability of moving m monomers at time t. u_m is the rate constant for adding a monomer to the segment of m monomers, and w_m is the rate constant for removing one monomer from the segment of length m. The rate constants are related by detailed balance, namely,

$$\ln \frac{u_m}{w_{m+1}} = -\beta(F_{m+1} - F_m). \tag{6}$$

If the rate constants are assumed to be independent of m, equation (5) can be transformed into continuum Smoluchowski (Fokker–Planck) equation. With this assumption, the mean

first passage time τ (i.e. the average time required by the chain to go from region I to II, after starting with at least one monomer in region II), can be solved, yielding [46]

$$\tau = \frac{1}{u} \int_0^N \exp(\beta F_{m1}) \, dm_1 \int_0^{m_1} \exp(-\beta F_{m2}) \, dm_2. \tag{7}$$

Using equation (7) Muthukumar calculated τ for several limiting cases of the chemical energy $\Delta\mu$ [43]. Of particular interest to the current review are the solutions for $\Delta\mu = 0$ (no potential), which yielded a quadratic scaling, $\tau \sim N^2$, and the strong-negative-bias limit, $\Delta\mu \ll 0$ (i.e. translocation along the direction of a strong electric field), which yielded a linear dependence, $\tau \sim N$. Experiments performed at 120 mV bias voltage support the linear scaling of τ with polymer length. The most probable translocation time, t_P, was measured as a function of N and displayed a linear dependence for DNA molecules longer than 12 nucleotides [19, 32]. This result is consistent with the prediction given for $\Delta\mu \ll 0$. In these measurements the electrical driving force was estimated to be roughly 50 pN, corresponding to an energy of $\sim 5k_B T$ per nucleotide length a (see below, section 3.4). This estimation is consistent with the limit $\Delta\mu \ll 0$ assumed in the model. It should be noted, however, that the asymmetric translocation time distribution observed in the experiments was not predicted by the model discussed above, making the comparison of τ with the experimental t_P less straightforward.

The simplified model described above was recently refined by introducing a third region that takes into account the finite thickness of a physical membrane and pore [47]. The free energy terms for the three regions with the corresponding mean first passage times were calculated for the cases of long and short polymers, with respect to the membrane thickness. The calculated results predict two kinds of translocation depending on the polymer size: for long polymers the translocation mean velocity, defined as the ratio of the polymer contour length and the average first passage time, approaches a constant value that does not depends on N; for short polymers, the velocity increases significantly with decreasing length. The transition between 'long' and 'short' is set by the thickness of the pore, d. These observations are in good agreement with experimental results discussed below.

3.3. Anomalous dynamics of polymer translocation

The Brownian polymer dynamics described above yielded a quadratic scaling of the first passage time with N in the absence of an external driving force. Chuang *et al* [48] noted that the time taken for a free polymer to diffuse a distance of the order of its radius by *Rouse* dynamics, scales with an exponent larger than two (self-avoiding polymer), which should provide a lower bound to the translocation time. Therefore, the quadratic scaling does not provide an accurate description of the process. To resolve the problem, numerical simulations of phantom and self-avoiding chains in one and two dimensions were performed.

The translocation problem was formulated in terms of a Fokker–Planck equation similar to the one described above, with respect to a single continuous coordinate, $s(t)$ (equivalent to $m(t)$ introduced in figure 5). The polymer dynamics was calculated using Monte Carlo simulations for one- and two-dimensional square lattices. The simulations started by placing the first monomer in the hole, while the remaining N^{-1} monomers are in a random conformation on the left side of the wall. The first monomer was not allowed to escape to the left. The simulation finished when the other end of the polymer passed through the hole, and the passage time was measured in units of Monte Carlo steps.

The most interesting results of these simulations were obtained in two dimensions: comparing the translocation process with simple diffusion, the polymer took a much longer
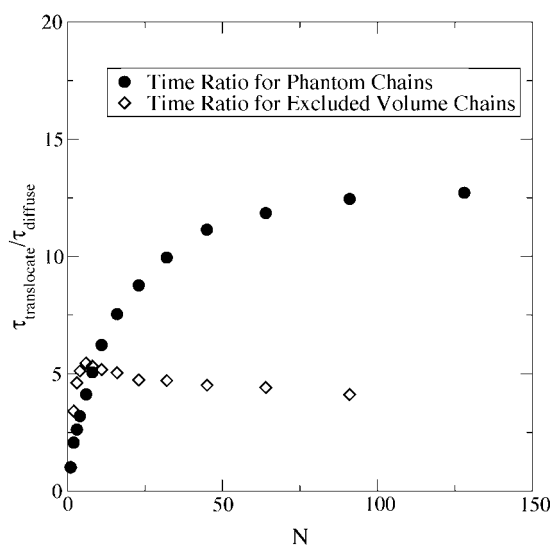
Figure 6. Comparison of simulation results for diffusion through a hole that may fit one monomer versus free diffusion over the same distance in the absence of a barrier. Translocation times through the hole are larger than the free diffusion for phantom and that for self-avoiding chains. In both cases, the ratio of these times levels off to a constant. This figure is after Chuang *et al* [48].

time to pass through the hole than the time it took for the polymer to freely diffuse the same distance. Defining the characteristic timescales as $\tau_{translocate}$ and $\tau_{diffuse}$ respectively, in both cases the same scaling with N was obtained, $\tau \sim N^{2.5}$ for a self-avoiding walk and $\tau \sim N^2$ for a phantom polymer. The slowing down of the polymer dynamics in the translocation case as compared to the free diffusion resulted from a much larger pre-factor for the translocation case (see figure 6). In the self-avoiding model (open symbols) the ratio between the pre-factors in the translocation versus the diffusion was ∼5 for polymers with $N \approx 5$ or longer and displayed a weak dependence on polymer length. The corresponding ratio for phantom polymers (solid symbols) approaches a constant value for $N \approx 60$ and higher.

The 'non-trivial' scaling presented above is expected to have consequences on the length dependence of the forced translocation velocity. The drift velocity u of a polymer due to a force F can be estimated as $u(F) \sim (R_g/\tau_r)\phi(FR_g/k_BT) \sim N^{\nu(1-z)}\phi(FN^{\nu})$ where ϕ is a scaling function that depends on the ratio of two quantities having dimensions of energy, R_g is the polymer's radius of gyration, and τ_r is its relaxation time [48]. If the velocity is proportional to the force, the scaling function ϕ must be linear in its argument and thus the mobility scales as $u/F \sim N^{-\nu(z-2)}$. In a similar way, the pulling velocity of the polymer *in the pore* can be approximated: $v \sim N/\tau\phi(\Delta\mu N/k_BT) \sim N^{2-z\nu}$. The anomalous slowdown due to Rouse dynamics leads to a mobility that scales as $N^{-0.18}$ in three dimensions. It is interesting to note that the assumption that the function ϕ is linear in its argument may not be valid for the translocation case, and in particular for strong driving forces. Indeed, the dependence of the translocation mean velocity was found to be quadratic in the applied electric field [19]. More experimental and theoretical results are needed in order to confidently claim that non-linearities could be intrinsic to the polymer dynamics in the pore, as opposed to non-linear dynamics resulting from polymer–pore interactions.

The translocation process of self-avoiding polymer dynamics in the presence of a driving field was also modelled using 3D Monte Carlo simulations by Chern *et al* [49], Kong *et al* [50],

and more recently by Loebl *et al* [51]. For their simulations Chern *et al* considered a thin wall with a thickness of the inter-monomer separation. Their results yielded a linear dependence of the mean first passage time on polymer length in accord with the analysis presented in section 3.2; however, the unrealistic dimensions chosen for the pore complicated the direct comparison of their results with experiments performed with the α-HL pore. In a more recent study, Loebl and his co-workers performed simulations with pore size and length chosen to be close to the experimental values, and studied the effects of temperature, voltage, and polymer length on the translocation time. A reasonably good agreement with the experimental results was obtained, but it was noted that the results strongly depended on the inter-monomer potential chosen for the simulations.

3.4. Calculations of polymer flux through the pore

Calculation of the total polymer flux through the pore involves the modelling of two processes:

(1) The 'capture' of a polymer end in the pore (involving diffusion of the polymers from the bulk to the vicinity of the pore and penetration of one of the ends into the pore).
(2) The dynamics of the polymer when it is partially (or completely) threaded through the pore (or polymer 'translocation') [32].

Because these processes are independent of each other, they can be characterized by two independent timescales: $\tau_{capture}$ and $\tau_{translocate}$ respectively. A low limit on $\tau_{capture}$ is set by the diffusion time in bulk $\tau_{diff} = 1/(DC_{bulk}^{2/3})$, with D the polymer diffusion coefficient and C_{bulk} its bulk concentration. $\tau_{translocate}$ is approximated by the apparent translocation duration, t_D. The polymer flux through the pore can be characterized by a rate, $R = \langle \delta t \rangle^{-1}$, equal to the inverse of the average time between translocation events. Depending on the rate-limiting processes in our system, δt can be bound by $\tau_{capture}$ or t_D (or both).

Ambjörnsson *et al* [52] have recently proposed a model that describes the dynamics of the polymer both inside and outside the pore. The model consists of a finite-width membrane placed parallel to the y–z plane, and a pore oriented in the x-direction. The length of the pore is denoted as d, and it extends toward the left side denoted as '*cis*'. The flexible polymer is modelled as a collection of connected points with a total contour length of L. Outside the pore the polymer is allowed to perform a random walk on a discrete lattice with lattice parameter a that is equal to the polymer's persistence length, and inside the pore the polymer's motion is restricted to one dimension. The polymer motion is expressed in terms of a single 'slow' variable m, similar to the one introduced above. The polymer flux $J(m, t)$ is related to the probability distribution function $P(m, t)$ described by a 1D Smoluchowski equation [52, 53], and a free energy term $F(m)$.

Using this description the polymer flux through the pore was obtained under two main assumptions:

(I) The friction coefficient inside the pore is uniform and additive (i.e. each of the polymers units in the pore contributes an equal amount, ξ).
(II) The electric field potential drop over the pore is linear, and is zero elsewhere.

For long enough polymers, analytical forms of the polymer flux are obtained:

$$J = J_0 f(g, V), \tag{8}$$

where g represents the entropy loss to confine N_P monomers in the pore ($N_p a$ equal to the pore length), V is the electrical potential, and J_0 is given by

$$J_0 = a_{pore} C_{bulk}/(R_g \beta \xi_P). \tag{9}$$

a_{pore} is a constant related to the pore geometry, C_{bulk} and R_g are the polymer bulk concentration and radius of gyration respectively, $\beta = 1/k_B T$, $\xi_P = N_P \xi$ is the total friction for the part of the polymer in the pore, and $f(g, V)$ is given by

$$f^{-1}(g, V) = \frac{V_c}{2V} \left\{ 1 + \gamma \sqrt{\pi} \exp(\gamma^2) \left[\mathrm{erf}\left(\sqrt{V/V_c} - \gamma\right) + \mathrm{erf}(\gamma) \right] \right\}. \tag{10}$$

Here $V_c = 2/N_P |q|\beta$ is roughly the electrostatic energy gain obtained by storing N_p polymer segments in a pore, $\gamma \equiv g/\left(2\sqrt{V/V_c}\right)$, and $\mathrm{erf}(x)$ is the error function. Assuming that $|q|$ is roughly equal to unit charge and $N_P \approx 12$ (see section 4), one obtains $V_c \approx 4$ mV.

The model predicted a free energy barrier for translocation (similar to the one presented in section 3.2) with height *and* width that were sensitive functions of the magnitude of the applied potential. Therefore, it was expected that the polymer flux would strongly depend on the voltage level. Four different regimes for the polymer flux as a function of V were distinguished:

(1) At very high field strengths the energy barrier vanished as compared to the thermal energy [52]. The threshold voltage for this regime was defined as $V_F \equiv g^2 V_c/4$. For $V > V_F$ the polymer flux was predicted to display a linear dependence on V.

(2) For intermediate field strengths ($V_{cross} < V < V_F$), finite-width and finite-height energy barriers were expected. The polymer flux was predicted to be well approximated by an exponential dependence on V. The lower limit for this regime, defined as $V_{cross} \equiv g V_c/2$, corresponded to the lowest value of the potential under which the flux was practically zero because the barrier width diverged. The value of V_{cross} was estimated to be ~ 40 mV by comparison to experiments.

(3) Below V_{cross} two separate regimes were distinguished ($V > V_c$ and $V < V_c$). Because for voltages smaller than V_{cross} the flux practically vanishes, these regimes are not accessible by experiments.

The exponential dependence of the flux on voltage in the intermediate range ($V_{cross} < V < V_F$) was verified in several experiments [32, 33, 54]. Moreover, the predicted crossover from an exponential dependence on V to a weaker dependence on voltage (roughly linear) was also observed in experiments discussed in section 4. Equations (8)–(10) were used to fit the translocation rate data measured over a broad voltage range and the values for V_c and g could be extracted and compared between different experiments. Using the fit values for g and V_c (see [52]), V_F was estimated as ~ 300 mV (at room temperature). We note, however, that at low polymer concentrations, bulk diffusion may set an upper limit on the measured rate, making the process diffusion limited and not process limited at high voltages.

3.5. A model for the polymer–pore interactions

A quantity of interest in the translocation experiment is the electrical force, F, driving the polymers through the pore. One can estimate F by assuming that each nucleotide in the DNA carries roughly one unit charge and therefore the electric energy gain for each nucleotide is eV. In this case, the force is $F \sim eV/a \approx 5k_B T/a$ (~ 50 pN) where $a \approx 4$ Å is the length of each nucleotide. It is interesting to examine whether hydrodynamic drag can balance this force. In a typical translocation experiment a voltage V of ~ 100 mV applied over the ~ 5 nm thick membrane results in polynucleotide translocation velocities of $v \sim 10^{-2}$ cm s^{-1} at room temperature [16, 18]. A rough estimate for the drag force inside the pore can be obtained by modelling the pore as a cylindrical hole of radius R and the moving polymer as a smaller cylinder with radius r. When the polymer moves with velocity v with respect to the pore
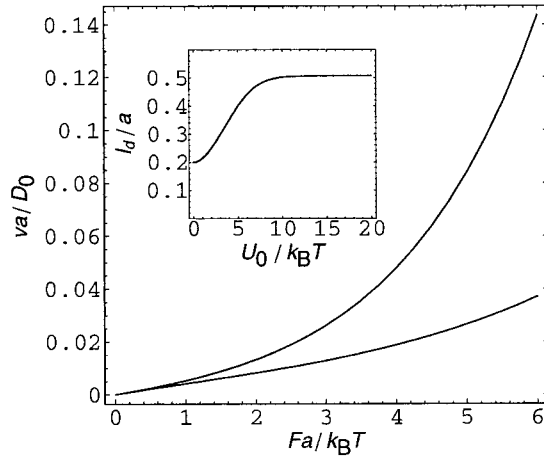
Figure 7. A plot of the dimensionless average velocity v versus the driving force Fa/k_BT, derived from a phenomenological microscopic model (sawtooth potential) of the interactions [40]. The parameter values are $U_0/k_BT = 10$, with $\alpha = 0.7$ for the upper curve and $\alpha = 0.3$ for the lower curve. The potentials are thus related by $U(x) \rightarrow U(-x)$. Inset: the diffusive length l_d versus the barrier height U_0 of the sawtooth potential, for fixed driving force $Fa = 5k_BT$ and asymmetry $\alpha = 0.7$. Note that over the entire range of U_0, $l_d \leqslant a$. This figure was adapted from [40] with permission.

the drag force per unit length is roughly $2\pi \eta r v/(R - r)$. For a DNA polymer moving inside the α-HL channel, $r/(R - r) \sim 2$ and therefore the force generated by hydrodynamic drag is $\sim 10^{-4} k_B T/a$, ~ 4 orders of magnitude smaller than F. It is also possible to show that the contribution to the drag force from the ends of the polymer outside the channel are 100 times smaller than F [40].

The arguments presented in the previous paragraph, together with experimental data suggesting that the translocation times depend strongly on the nucleotide type [17, 18], imply that polymer–pore interactions, rather than the more generic hydrodynamic drag, play an important role in determining the translocation dynamics. Motivated by this evidence, Lubensky and Nelson [40] proposed a phenomenological 'microscopic' potential, $U(x)$, to describe the polymer–pore interactions. Their potential has the shape of an asymmetric sawtooth characterized by three parameters: the period, a (chosen to be equal to the polymer unit length), the distance between one minimum and the next maximum, αa, and the potential height, U_0. Ignoring the contribution of the parts of the polymer outside the pore, and focusing only on the parts inside the channel, the problem is formally no different from that of a point particle diffusing in the potential $U(x)$ and driven by a constant force F. The probability $P(x)$ of finding such a particle at a point x is governed by a Smoluchowski equation:

$$\frac{\partial P}{\partial t} = D_0 \frac{\partial}{\partial x}\left[\frac{\partial P}{\partial x} + \frac{U(x)/a - F}{k_B T}P\right]. \tag{11}$$

The bare diffusion constant D_0 is related to the hydrodynamic drag force and should not be confused with the effective diffusion constant, D, introduced in equation (2), which includes the potential effects and describes the motion of the polymer on length scales much larger than a.

Using the model potential described above, Lubensky and Nelson solved equation (11), and obtained limiting expressions for D and v as a function of the force and the potential strength. Their main results are depicted in figure 7. In the main figure the dimensionless

velocity is plotted against the driving force. The two curves correspond to different values of the asymmetry factor, α: 0.7 for the upper curve and 0.3 for the lower curve. As expected, the drift velocity increases with the force in both cases. The difference between the two lines illustrates the significance of the potential barrier height in each step: a tilt of the asymmetric potential leads to a small barrier for the $\alpha = 0.7$ case and to a large barrier for $\alpha = 0.3$. More interesting are the results for the diffusive length l_d ($=D/v$) as a function of the potential height U_0 (inset): even when U_0 was varied over a large range, l_d only varied from ~ 0.2 at very small potential strengths to 0.5 at strong potentials. Although the effective diffusion and the drift velocity separately can depend strongly on U_0, their ratio, l_d, is far less sensitive.

The typical values of l_d obtained from the model ($\sim 0.3a$) cannot account for the much higher value estimated from the width of the translocation distribution discussed above ($\sim 40a$). A possible source for the inconsistency between the model's predictions and experimental results is the point-like nature of the translocating molecule, considered in the model, as opposed to the long polymers used in experiments. It is plausible to assume that the interaction between the polynucleotide and the 5 nm long channel takes place in multiple points along the channel simultaneously, rather than in one point. This assumption is supported by measurements displaying strong increase of polymer velocity for polymers shorter than 5 nm [19]. Thus, a chain made of connected particles such as the one considered above may interact more strongly with the channel especially if cooperative effects are allowed. This may result in significant broadening of the expected translocation distribution measured by $\delta t_P/t_P$.

The theoretical models presented above capture the main ingredients of the translocation process. The experimental results suggest that polymer–channel interactions predominantly determine the polynucleotide transport in the pore. This point is discussed in section 4 below. However, when comparing the experimental results to the models, it is apparent that point particle interactions are not sufficient and that the polymer nature of the molecules needs to be considered for a more realistic description of the problem.

4. Experimental section

In this section we review experiments in which the transport of ssDNA and RNA through the pore was studied. This process can be separated into two essential steps: first one end of the polynucleotides must enter the pore directed by diffusion and by the action of the local electric fields near the pore. Second, the molecules are translocated from one side of the membrane to the other, driven by the electric field potential across the membrane. The experimental section thus consists of two main parts. In the first part, experiments related to the rate of polymer entry to the pore measured by the time between events (see figure 3) are discussed. In the second part experiments probing the dynamics of the polynucleotides while inside the pore are described. We focus on three aspects of the problem: the sensitivity of the translocation process to polynucleotide–channel interactions, to polymer length, and to the applied electric field.

4.1. The rate and the probability for polynucleotide entry

Prior to translocation, the polynucleotide must be transported to the pore and one end of the molecule's ends must enter. We call this process polymer 'capture'. We will consider first the *distribution* of times elapsed between successive captures, $P_0(\delta t)$. Meller and Branton [32] derived a simple form for this distribution under two simplifying assumptions:

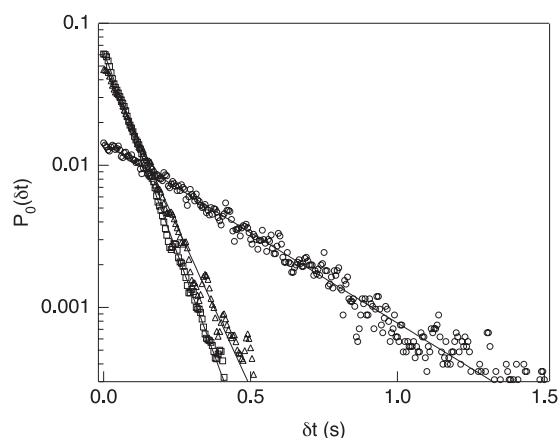(1) The capture rate is not diffusion limited (i.e. the polymer bulk concentration is high enough).

Figure 8. Normalized distributions of the elapsed time between successive capture events, δt. Three polymer types are displayed: $(dA)_{20}$ at 2.3 μM (squares); $(dCdCdTdCdC)_6$ at 1.8 μM (triangles); $(dC)_{40}$ at 0.5 μM (circles). The distributions are obtained from measuring at least 5000 values of δt for each sample. In each case the distributions are normalized by the total number of events. The solid lines are exponential fits (see the text) that can be used to extract the averaged event rate and its error (13.05 ± 0.55, 10.45 ± 0.52, 2.93 ± 0.14 s^{-1} for the three polymers respectively). Scaling the rate values by the corresponding bulk concentration, one obtains a single value, 5.8 ± 0.1 s^{-1} μM^{-1}, supporting a linear scaling of the rate on C_{bulk}. This figure was reproduced from [32].

(2) At the same time the bulk concentration (and in particular near the pore) is low enough that polymer–polymer correlations can be ignored.

Deviations from the simple prediction may indicate that these assumptions were not accurate.

For dilute samples one can assume that the average capture rate R is stationary. We allow R to depend on the concentration of polymer in bulk, C_{bulk}, the pore entrance area, A, the applied electric voltage, V, and the temperature, T. The probability of observing zero capture events, P_0, at time t measured from the occurrence of the last event is given by $P_0 = (1 - R\,\Delta t)^{t/\Delta t}$ for an arbitrarily small time slot Δt. Taking the limit $\Delta t \to 0$ we obtain

$$P_0(Rt) = e^{-R(C_{bulk}, A, V, T)t}. \tag{12}$$

The simple exponential prediction given by equation (12) was tested for different polynucleotide types and concentrations [32]. The elapsed time between events was measured at 120 mV as explained in figure 3. At least 5000 events were obtained at each condition. Figure 8 displays the semi-log distribution of δt, measured for three different polymer types at different concentrations and at $V = 120$ mV. In these experiments and in others not shown here, the data are well fitted by a single exponential function over more than two decades. The average capture rates, R, and their errors were extracted from the fits in the three experiments and were found to be 13.05 ± 0.55 s^{-1} for poly$(dA)_{20}$, 10.45 ± 0.52 s^{-1} for poly$(dCdCdTdCdC)_6$, and 2.93 ± 0.14 s^{-1} for poly$(dC)_{40}$. By normalizing these values by the corresponding DNA molar concentrations of the three samples (2.3, 1.8, and 0.5 μM), a single value was obtained: 5.8 ± 0.1 s^{-1} μM^{-1}, suggesting a linear scaling of R in C_{bulk}. The normalized capture rate was weakly dependent on the type of DNA, but it strongly depended on the electrical potential as discussed later. We note that for the data displayed in figure 8, no deviation from the exponential dependence was observed, even at short times.

The event rates reported above can be compared with the limit set by bulk diffusion: for a typical bulk concentration of $C_{bulk} = 1$ μM and diffusion coefficient $D = 10^{-7}$ cm^2 s^{-1},

the average diffusion time $\tau_{diff} = 1/(DC_{bulk}^{2/3}) \sim 1$ ms. This value corresponds to a theoretical maximum event rate of ~ 1000 s^{-1}, much higher than the typical rates obtained in the experiments reported above. This analysis supports the assumption that R was not diffusion limited (at the experimental conditions used above). Because the capture rate is much lower than the reciprocal value of τ_{diff}, we expect that molecules will 'collide' with the pore more often than they are captured. Indeed, in experiments one observes short current spikes as well as full translocation blockades. The time duration of these spikes is set by the response time at the electrometer (and not by polymer type), which is of the order of few microseconds. On choosing appropriate conditions (set by temperature, voltage, polymer length, etc), the translocation time, t_D, satisfies $t_D \gg \tau_{inst}$, where τ_{inst} is the system response time[2], and the short spikes can be readily distinguished from 'true' events.

Henrickson *et al* [33] compared the averaged capture rate for DNA entry into the pore from the '*cis*' side and from the '*trans*' side and at different DNA concentrations. Their results suggest that for a given DNA concentration, polymers added to the '*cis*' side are six times more likely to be captured than polymers added to the '*trans*' side. The results were rationalized by the possible electrostatic repulsion between the DNA and the pore and a higher entropic barrier for entering from the '*trans*' side, as opposed to an electrostatic attraction and lower entropy barrier expected for entry from the '*cis*' side. The rate of polymer capture from both sides was linear with the corresponding bulk polymer concentration.

The dependence of the capture rate on the applied voltage was explored by three different groups. Henrickson *et al* measured the dependence of R on the applied voltage in the range 55–120 mV for poly(dC)$_{30}$ at room temperature. In this range the data were well approximated by an exponential function. Nakane *et al* [54] have extended the voltage range from 100 to ~ 300 mV and found a roughly linear relationship between R and V for $V > 200$ mV, measured for poly(dA)$_{50}$. Meller and Branton [18] took advantage of the discovery that the DNA translocation (characterized by t_D) is considerably slowed down at low temperatures. Therefore even at high voltages, where t_D is significantly shortened [19], the relationship $t_D \gg \tau_{inst}$ still applied, facilitating the discrimination between real translocations and the collision spikes.

Figure 9 displays the dependence of the capture rate measurements of Meller and Branton [32] for the voltage range 60–250 mV, measured at $T = 2\,°C$. Looking first at the semi-log plot of R versus V (inset) we see that the two data sets for poly(dC)$_{40}$ at 2.6 μM (circles) and 0.9 μM (squares) display an exponential increase with V for the low-voltage range (60–140 mV) with a similar slope (0.075 mV^{-1}). Above ~ 150 mV we observe a crossover to another regime. In the high-voltage regime the slope of the data in the semi-log plot is ~ 5 times smaller than in the low-voltage regime. The solid curves are three-parameter fits (V_C, g, J_0) to the polymer flux predicted by Ambjörnsson and co-workers [52] (see equations (8)–(10)). The fit yielded J_0-values that compare well with measurements done at room temperature (poly(dC)$_{30}$) [52]. The data are also shown on a linear scale plot to illustrate the quality of the fit.

The transition from the exponential dependence on V to the approximately linear regime was predicted to occur at $V_F \equiv g^2 V_c/4$. Plugging in the values that we obtain by fitting the data ($g = 20$, $V_C = 3.2$ mV; see figure 9), one finds $V_F = 320$ mV. In comparison, the crossover in the capture rate data occurs at roughly 150 mV. The discrepancy could be related to the approximations involved in the model and in particular the assumptions that the electric field distribution inside the pore is uniform and that there is a constant friction term inside the

---

[2] The system response is usually set by a low-pass filter, characterized by its rise time $T_r \approx 0.332/f_C$ where f_C is the filter's corner frequency [55]. For a 100 kHz Bessel filter, $T_r \approx 3.3$ μs.
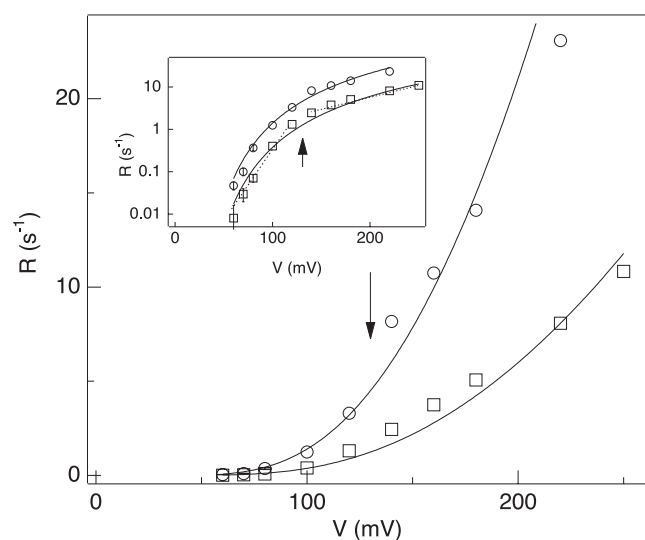
Figure 9. The capture event rate, R, measured at $2\,^\circ$C using the method described in figure 8, as a function of the applied voltage V in the range 60–250 mV. The polynucleotides used in this experiment were $(dC)_{40}$ at 2.6 μM (circles) and at 0.9 μM (squares) at the *cis* chamber. The inset displays the data on a semi-log plot showing that a single exponential (straight line) cannot account for the data over the entire voltage range. The arrows indicate the crossover regions. The solid curves are fits according to the prediction of Ambjörnsson *et al* [52] (equations (8)–(10)), yielding $V_C \approx 3.3$; $g \approx 20$ and $J_0 \approx 4.2$ and 1.4 for the two polymer concentrations respectively. To compare the J_0-values at room temperature with those measured at $2\,^\circ$C, we use equation (9) and we estimated the ratio of the friction coefficients ξ at the two temperatures from the ratio of the translocation time, t_P of these polymers measured separately (data not shown). The scaled J_0-values (at room temperature) are 38 and 12.3 for the high and low concentrations respectively. The data were reproduced from [32].

channel. It is encouraging, however, that equation (8) approximates the data fairly well over the entire voltage range that spans ~3 decades in the rate values.

4.2. The dynamics of polynucleotide translocation

The discovery that the electrical field can drive the translocation of ssDNA and RNA molecules through the α-HL pore [16] set the stage for a variety of experiments in which the influence of physical parameters such as temperature, voltage, and polymer length, as well as the DNA and RNA structures and sequences, were examined. In this section we review some experiments undertaken to characterize the dynamics of the polynucleotides' translocation process. We discuss three main results:

(a) The translocation duration is highly sensitive to the polynucleotide sequence (ssDNA and RNA) and secondary structure (RNA).
(b) The translocation duration as a function of polymer length.
(c) The non-linear dependence of translocation duration on V, and the dynamics of polynucleotides at vanishing electric field.

4.2.1. The dynamics of polynucleotides in the α-HL pore is highly sensitive to RNA secondary structure and DNA–protein interactions. Akeson and co-workers [17] compared the translocation blockade signals among RNA homopolymers and their ssDNA analogues.
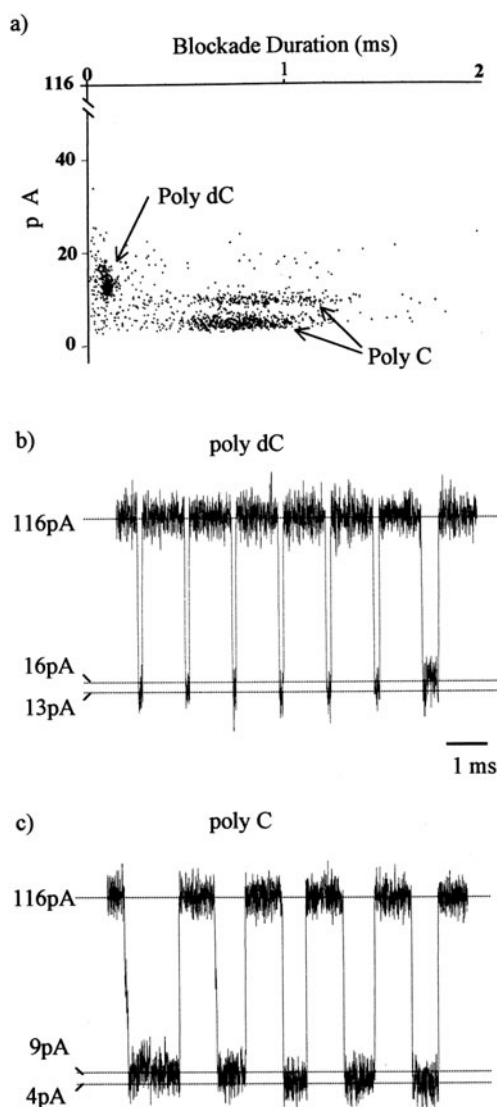
Figure 10. Comparison between poly(C) and poly(dC) current blockades. The poly(C) was a strand of 130 ± 20 nucleotides (nominal length); the poly(dC) was a 100-mer. (a) The event diagram, in which each point corresponds to the measured I_B and t_D caused by a single polynucleotide passing the α-HL pore. Note the large time dispersion of the poly(C) events as compared to the poly(dC) ones. ((b), (c)) Typical blockades caused by the poly(dC) and poly(C) molecules used in (a) above. The data in these experiments were digitally filtered at 50 kHz. Quiescent periods between events were spliced out so that several blockades could be presented. This figure was adapted from [17] with permission.

Specifically, the blockade signals were obtained from polycytidylic acid (RNA) and polydeoxycytidylic acid (ssDNA), of comparable lengths (see figure 10). Looking at the figure, three main features are easily discerned:

 (1) The translocation duration, t_D, of poly(dC) is much shorter than that of the poly(C) (roughly 0.9 versus 5.8 μs/base).

(2) The blockade events of the poly(dC) polymers yielded a single, tight, cluster of events on the translocation diagram (see figure 10), whereas the poly(C) events are organized in two clusters spread over a large range in t_D (roughly 500–1300 μs).

(3) The blockade current of the poly(C) is lower than the corresponding current for poly(dC) ($\sim$7 versus $\sim$14 pA respectively).

The remarkable differences between the two molecules were rationalized by the idea that secondary structure existing in the poly(C) molecules and not in the poly(dC) might be responsible for the different behaviour: poly(C) molecules have a strong tendency to form single-stranded helices $\sim$1.3 nm in diameter [56] with a structure narrow enough to traverse the pore, causing larger blockades than those in the less structured poly(dC). It was also found that the unstructured polyuridylic acid (poly(U)) translocated at rates similar to the poly(dC), at roughly 1.4 μs/base.

In another set of translocation experiments, Meller and his co-workers [18] investigated the properties of a variety of single-stranded DNA molecules at different temperatures. One of the striking results of this study was the large difference between the characteristic translocation time of polydeoxyadenylic acid (poly(dA)) and polydeoxycytidylic acid (poly(dC)). In figure 11(a), a t_D versus I_B event diagram is displayed for the separately examined poly(dA) (black/blue markers) and poly(dC) (grey/red markers). Each point on this diagram represents a single translocation event with corresponding values of t_D and I_B. The two polymer types form two well separated groups of events, mainly because of the significant difference in their translocation times. The most probable translocation time, t_P, for each of the polymers was determined from the translocation time distributions (figure 11(b)) measured separately for each polymer, yielding 1.2 μs/base for poly(dC), and 3.3 μs/base for poly(dA).

A representative set of ten translocation events measured from an equal molar *mixture* of poly(dA)$_{100}$ and poly(dC)$_{100}$ is shown in the lower panel of figure 11. The translocation duration of each event was measured 'on the fly' and is labelled on top of each event. Because of the big separation in the characteristic translocation time distributions, it was possible to identify the type of each molecule as it exited the pore [18].

The nearly threefold difference between the t_P-values of the two polymers has a weak dependence on temperature and in particular is maintained at elevated temperatures (up to 40 °C) [18]. Poly(dA) molecules have a higher tendency to form single-stranded base-stacked helices as compared with poly(dC). However, base stacking interaction is expected to be less stable at higher temperatures, and therefore the weak dependence of the ratio $t_P(dA)/t_P(dC)$ on temperature suggests that in the DNA case base stacking (or secondary structure) alone cannot account for the differences in t_P-value of the two polynucleotides.

Further evidence showing that the base stacking alone in the ssDNA polymers cannot account for the strong shift in the translocation time was obtained by comparing t_P among polynucleotides with varying numbers of adenines evenly spaced in cytosines polymers. The association constant of dA–dC stacking is less than half that of the dA–dA stacking [57]. If base stacking interactions were a predominant factor that limited the DNA translocation speed, and thus increased t_P, we would expect polymers with contiguous sequences of adenines to translocate more slowly than polymers with adenines interspersed within cytosines. The result showed the opposite trend (figure 12): a few evenly spaced single adenines in a predominantly cytosine polymer markedly slowed polymer translocation. This point is most prominently illustrated by comparing 0% dA's point that yielded $t_P = 150$ μs with the 10% dA's point that yielded $t_P = 230$ μs. The addition of a single dA base interspersed by nine dC bases resulted in an increase of 150% in t_P.
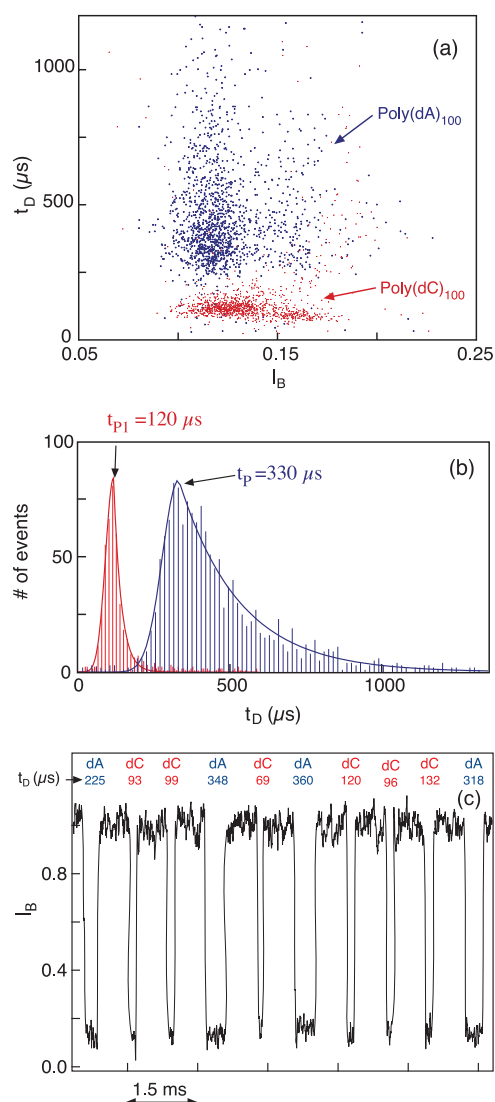
Figure 11. (a) The event diagram of poly(dA)$_{100}$ (black/blue markers) and poly(dC)$_{100}$ (grey/red markers). Each spot represents translocation of a single molecule characterized by its t_D and the normalized blockade current, I_B (defined as the average current during translocation divided by the open pore current). The two polymer types form two well separated groups of events, reflecting the ~3-fold difference in the peaks of their translocation distributions. (b) The translocation duration distributions were constructed from the t_D of more than 1000 events for each polymer type. These distributions are characterized by the most probable translocation time, t_P, and are well approximated by fast-growing Gaussians for $t_D < t_P$ and falling exponentials for $t_D > t_P$. (c) Representative current blockade traces of ten events recorded from a *mixture* of equal molar concentrations of poly(dC)$_{100}$ and poly(dA)$_{100}$. The translocation duration is given in microseconds for each event. The clear difference between the t_D of the two equal-length DNAs permitted discrimination of the two molecules in the mixture. The data were acquired at $20.0 \pm 0.1\,^{\circ}\mathrm{C}$ with a 100 kHz low-pass filter, digitized and analysed at 333 kHz/12 bits. For the display the data were digitally low-pass filtered at 10 kHz ((c) only), and the quiescent periods between events were spliced. The data were reproduced from [18].

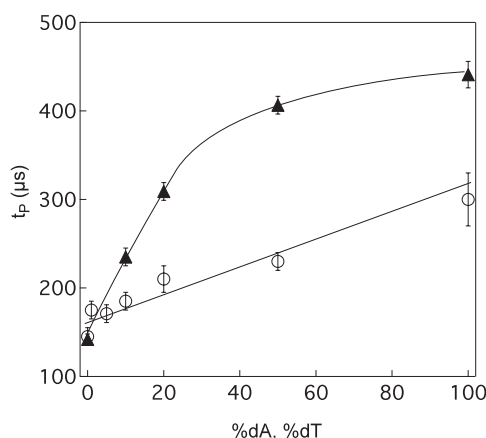(This figure is in colour only in the electronic version)

Figure 12. The effect of purines (dA) and pyrimidines (dC and dT) on translocation times. The most probable translocation time, t_P, was obtained from the translocation distributions as in figure 11(b), for a set of 100-mers with evenly spaced dAs or dTs in poly(dC) polymers. Because the minority population of deoxynucleotides was evenly spaced in the polymer, when fewer than half of the deoxynucleotide are adenines or thymines, no self-stacking of these bases can occur. The fraction of adenines (solid triangles, $T = 17.5\,°C$) or thymines (open circles, $T = 18.0\,°C$) is denoted as a percentage. If purine base stacking was a predominant determining factor of t_P we would expect the addition of small evenly spaced dAs not to change t_P significantly, and over 50% dAs a significant shift would be seen. The result is the opposite to this expectation (see the text), implying that dA base stacking is not a predominating factor affecting t_P. This figure was adapted from [32].

The addition of a few adenine bases in an otherwise pure poly(dC) polymer induces a notable increase in t_P but is not expected to significantly change the persistence length of the polymer. Therefore the entropic contributions to the translocation process discussed in section 3 are likely to be similar. On the other hand, if adenines favourably interact with pore residues as compared with cytosines, even a small addition of dAs could result in a significant increase in t_P.

To summarize, for the case of RNA homopolymers the translocation dynamics in the α-HL pore was greatly affected by the local structure of the polynucleotides [17]. In the DNA case the dynamics was mostly dominated by nucleotide–pore interactions, which is base specific, in particular for the case of poly(dC) and poly(dA). Going back to the translocation duration distributions displayed in figure 11(b), the long decaying tail for $t_D > t_P$ could be a result of these interactions. Approximating these decays by exponential functions, the ratio of the characteristic timescale for poly(dA) and poly(dC) is $\sim$7 [18]. This value is significantly larger than the corresponding t_P-ratio of the two polynucleotide types illustrating how DNA–pore interactions affect the polymer dynamics in the pore.

4.2.2. The dependence of polymer translocation on polymer length. Measurements of the mean translocation time of polyuridylic acid (poly(U)) in the range 100–500 nucleotides and at $V = 120$ mV, appeared to be linear with N [16], in agreement with the energy barrier model presented in section 3.2. More recently, the dependence of t_P on polymer length was examined for shorter polynucleotides in the range 4–100 bases [19, 32]. Polymers longer than $N = N_P = 12$ bases were found to obey the linear dependence on length regardless of their sequence. This result supports the idea that the enthalpic term (polymer–DNA interactions) for long polymers has a weak dependence on N. In contrast, for $N < N_P$ the translocation time was found to decrease with decreasing N in a non-linear way. Because the transition between the long and short regimes was abrupt and not gradual, and because the deflection
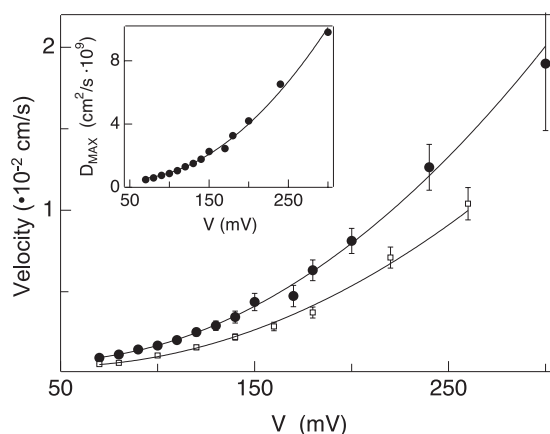
Figure 13. The dependence of the average polymer velocity defined as $\bar{v} = L/t_P$ on the applied voltage V is not linear. Data are shown for $(dA)_{12}$ (solid circles) and $(dA)_{30}$ (empty squares) measured at $2\,°C$. The solid curves are quadratic fits of $\bar{v} \sim (V - V_0)^2$ to the data, with $V_0 \approx 47 \pm 8$ mV being the minimal potential required to support translocation extracted from the fit. Inset: estimated upper bound values for the effective polymer diffusion coefficient inside the pore based on $\bar{v}$. This figure was adapted from [19].

point ($N = N_P$) corresponded to a polymer contour length of $\sim$5 nm (which is also the channel length), it was concluded that in the short-polymer limit the magnitude of the DNA–protein enthalpic interaction does depend on N [19]. If, for example, the number of contact points contributing to the total interaction between the polymer and the pore is proportional to N (for $N < N_P$) and the combined enthalpy is assumed to be additive, on average shorter polymers will experience smaller interactions, and thus display a sharp decrease in t_P.

The Brownian free energy barrier model described in equations (4)–(7) above predicted a quadratic scaling of the translocation time in N, $\tau \sim N^2$, for the case of $\Delta\mu = 0$ (zero chemical energy), and a linear scaling, $\tau \sim N$, for the case of strong negative bias ($\Delta\mu \ll 0$). The linear scaling with N is in line with the experimental results for long polymers. The simple model fails to describe the transition described above for $N < N_P$. This is not surprising, since this model does not take into account the finite length of the channel, d, and therefore it should not be considered for polymers shorter than d.

More recently a relatively simple refinement to the energy barrier model was accomplished by introducing a third region that takes into account the finite thickness of a physical membrane and pore [47]. The free energy terms for the three regions with the corresponding mean first passage times were calculated for the cases of long and short polymers, with respect to the membrane thickness. These calculations predicted two kinds of translocation depending on the polymer size: for long polymers (and for $\Delta\mu \ll 0$), $\tau \sim N$ as before; but for short polymers, τ decreased with a stronger dependence on N as compared to the long-polymer case. These results were in good agreement with the experiments described above, and the transition between 'long' and 'short' was set by the thickness of the pore, d, corresponding to polymer length $N \approx N_P$.

4.2.3. The dependence of polymer translocation on the electric field strength. The dependence of t_P on the applied electric voltage, V, was measured for polymers above the transition point ($N = 30$) and close to the transition ($N = 12$) [19]. In order to compare the two data sets and cancel out the linear dependence on polymer length discussed above, the
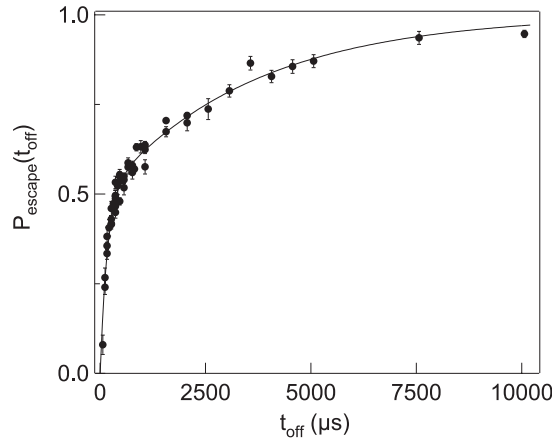
Figure 14. The dynamics of the polynucleotide inside the pore can be measured at zero applied voltage ($V = 0$) by drawing the polymers inside the pore for a given time, t_{drive}, and then measuring the probability that the polymer will escape from the pore after a period t_{off} in which no voltage is applied. This probability as a function of t_{off} displays two clear timescales one of which is remarkably long. For these experiments, $(dA)_{60}$ polynucleotides were used at $T = 15\,°C$, with t_{drive} fixed at 200 μs. Each data point was evaluated from ~ 1000 event recordings. The solid curve is a three-parameter fit to a sum of two exponents. The fast and slow timescales obtained from the fit are 165 ± 10 and 3500 ± 250 μs respectively, with a relative weight factor of 0.49 ± 0.01. The multiple data points at the same t_{off}-values represent measurements repeated using the same parameters. This figure was adapted from [58].

mean translocation velocity was calculated by dividing the polymer length by the translocation duration: $\bar{v} = Na/t_P$, where a is the polymer unit length. The dependence of $\bar{v}$ on the voltage is displayed in figure 13. Over the entire voltage range the data were well approximated by a quadratic dependence on voltage: $\bar{v} \sim (V - V_0)^2$, where $V_0 \approx 47 \pm 8$ mV represented the minimal potential required to support translocation as extracted from the fit. Using this value, one can estimate the electrical energy associated with introducing $N = N_P$ bases into the pore. Assuming one unit charge per base we get $e(V_0/d)a \sum_{n=1}^{N_P} n \approx 12 k_B T$. Because the effective charge on DNA is less than a unit charge, this value should be considered as a rough upper estimate to the entropy loss of introducing 12 bases into the pore.

Because of the observed non-linear dependence of the translocation velocity on voltage and the predicted even stronger scaling of the mobility in N at $\Delta\mu = 0$ (see section 3.3), it is interesting to probe the dynamics of the polymers at zero field ($V = 0$). However, the current blockade mechanism underlying the Coulter counter approach described above relies on measuring the residual ionic current during polymer translocation, which is proportional to V. Therefore it does not work at zero field. A method for overcoming this shortcoming was recently realized and implemented by Bates and co-workers [58]: the polymers were driven into the pore, using the same principles as described above, for a fixed time, denoted t_{drive}. After that time the applied voltage was set to zero and the system was allowed to evolve for a variable time, t_{off}. The probability of finding the polymer in the pore was measured at the end of the t_{off}-period, by applying a small 'probing' voltage (~ 40 mV), repeating the experiment many times and constructing an appropriate histogram.

These experiments yielded *two* characteristic timescales associated with the molecule transport from inside the pore to outside (or polymer 'escape'), instead of a single timescale (figure 14): the shorter timescale was attributed to the unhindered DNA transport from the pore, and the long timescale was attributed to molecules interacting with pore residues, and

thus being held in the pore for milliseconds. The ratio of the two timescales was roughly 21, measured for poly(dA) polynucleotides. It is interesting to notice that the long timescale value was found to be sensitive to the polymer sequence, whereas the short timescale was not. In particular, the poly(dC) yielded a shorter long timescale and similar short timescale [59]. It was also demonstrated that the slow timescale was highly sensitive to the applied electric field.

The discovery that at very low or zero electric field strengths some polynucleotides can stay in the pore for very long times and some escape from the pore much more quickly could be accounted for if the long timescale was dominated by the unbinding kinetics of the polynucleotides to the pore [58]. Thus at zero electric field the kinetics of DNA binding to the pore can be estimated. In contrast, at the high electric field values typically obtained in the translocation experiments, the interaction potential is strongly biased by the field in a similar way to that pictured by Lubensky and Nelson (see section 3.4), yielding a relatively complex translocation time distribution, for which one of the prominent features was the long tail at long times (see figure 11(b)). It remains to be understood how the tilt in the potential produces a quadratic dependence of the drift velocity on the voltage, as opposed to the linear response predicted by theory.

5. Conclusion and summary notes

The blockade signals produced by single polynucleotides traversing narrow pores contain useful information about the polymer dynamics. The interactions of different types of nucleic acid with the protein channel residues can slow down the translocation process in a base-specific manner. For short polymers ($N < N_P$), these interactions dominate the polynucleotide transport. For longer polynucleotides ($N > N_P$), enthalpic pore interactions and entropic contributions from the polymer outside the channel should not be neglected. The electrical field induces a strong shift in the potential and results in a non-linear dependence of the average polymer velocity, $\bar{v}$, on the applied voltage, V, that is well approximated by $\bar{v} \sim (V - V_0)^2$. Theoretical models and computer simulations of polymer dynamics in the pore are in many cases consistent with the experimental results, and provide insight into the underlying physical laws governing polymer transport through pores.

This review is a short summary of the growing body of experimental and theoretical efforts undertaken to study polymer transport through the α-HL channel and related questions. The focus of this article is on experiments and theoretical results directly related to polymer dynamics in the pore. As was delineated in the introduction, nanopores have a number of potential applications as biosensors, and as a novel means of analysing biopolymers. We anticipate that a better understanding of the physics and chemistry (dynamics and interactions) underlying biopolymer transport through narrow pores would set the stage for further and improved applications in the life sciences. For example, nanopores have been recently proposed as a novel means for sequencing unlabelled single DNA molecules [60–62], and for the detection of single-nucleotide polymorphism (SNP) [63].

Experiments involving biopolymer translocation through the alpha-haemolysin protein pore constitute the bulk of the results presented in this review. α-HL is a robust complex with a well characterized crystal structure. However, some applications will benefit from structures and chemical robustness not offered by the α-HL. For example, it is highly desirable to control the limiting aperture size of the nanopore and its aspect ratio. Since the current blockade magnitude is roughly proportional to the volume occupied by the polymer divided by the channel volume [19, 20], the information encoded in the current traces is averaged over a length scale of the order of the channel length ($\sim$5 nm in the case of α-HL). An atomically sharp aperture may, in principle, maximize the current read-out resolution, because

the blockades will be sensitive to a single monomer in the translocating polymer. Efforts to develop a solid-state, atomically sharp, nanopore are under way. Using a focused ion beam technology followed by an Ar^+ ion bombardment, Li *et al* [64] have recently produced pores in Si_3N_4 membranes with a diameter of a few nanometres. Preliminary experiments demonstrated that these solid-state pores could be hydrated and could be used to detect the passage of DNA molecules using the ion current blockade principal. Other efforts to fabricate nanopores in organic substrates are also in progress [65].

An alternative approach to circumvent the limits imposed by the α-HL involves the use of genetic engineering in order to modify protein channels such as the α-HL and others to introduce features not existing in the wild-type proteins. One of the aspects that make this approach highly attractive is the minuscule marginal cost of production of a mutant protein (per unit) once the desired form has been determined. The underlying ideas behind this approach were summarized in a paper by Bayley and Cremer [26].

Understanding the factors governing polymer dynamics inside nanoscopic channels can provide useful insights for future applications of the nanopore concept. One of the goals of this review is to delineate how basic research in this field directly impacts potential applications of the nanopores as bioprobes. As an example, we consider the prediction discussed above that an atomically sharp or 'ideal' aperture would produce a read-out with higher resolution than the one produced by the 5 nm α-HL pore. In this article we have reviewed results showing that the translocation speed is strongly impeded by *interactions* between the channel and the polynucleotide. An 'ideal' aperture would present minimal hindrance (because of its small cross-section) of the translocating molecule. In combination with the fact that the electric field intensity in the pore area may be $\sim$50 times larger than the estimated field strength across biological membranes (for the same applied voltage), this would result in an extremely fast translocation velocity. Since the blockade experiments rely on the measurement of the residual ionic current per base during translocation, the signal/noise ratio will be diminished. This example illustrates how further theoretical and experimental efforts in the field are likely to provide extremely useful insights into the development of better applications that make use of nanopores.

Acknowledgments

References

[1] Lodish H, Baltimore D, Berk A, Zipursky S L, Matsudaira P and Darnell J 1996 *Molecular Cell Biology* (New York: Freeman)
[2] Hille B 1984 *Ionic Channels of Excitable Membranes* (Sunderland, MA: Sinauer Associates, Inc.)
[3] Bezrukov S M 2000 *J. Membr. Biol.* **174** 1–13
[4] Schatz G and Dobberstein B 1996 *Science* **271** 1519–25
[5] Driselkelmann B 1994 *Microbiol. Rev.* **58** 293–316

[6] Kokjohn T A 1989 *Gene Transfer in the Environment* ed S B Levy and R V Miller (New York: McGraw-Hill) pp 73–97

[7] Ippen-Ihler K 1989 *Gene Transfer in the Environment* ed S B Levy and R V Miller (New York: McGraw-Hill) pp 33–72

[8] Miller R V 1998 *Sci. Am.* **278** 67–71

[9] Bustamante J O, Oberleithner H, Hanover J A and Liepins A 1995 *J. Membr. Biol.* **146** 253–61

[10] Whittaker G R and Helenius A 1998 *Virology* **246** 1–23

[11] Kasamatsu H and Nakanishi A 1998 *Annu. Rev. Microbiol.* **52** 627–86

[12] Salman H, Zbaida D, Rabin Y, Chatenay D and Elbaum M 2001 *Proc. Natl Acad. Sci., USA* **98** 7247–52

[13] Hanss B, Leal-Pinto E, Bruggeman L A, Copeland T D and Klotman P E 1998 *Proc. Natl Acad. Sci., USA* **95** 1921–6

[14] Mitchell P 2001 *Nat. Biotech.* **19** 717–21

[15] De Gennes P G 1979 *Scaling Concepts in Polymer Physics* (Ithaca, NY: Cornell University Press)

[16] Kasianowicz J, Brandin E, Branton D and Deamer D 1996 *Proc. Natl Acad. Sci., USA* **93** 13770–3

[17] Akeson M, Branton D, Kasianowicz J, Brandin E and Deamer D 1999 *Biophys. J.* **77** 3227–33

[18] Meller A, Nivon L, Brandin E, Golovchenko J and Branton D 2000 *Proc. Natl Acad. Sci., USA* **97** 1079–84

[19] Meller A, Nivon L and Branton D 2001 *Phys. Rev. Lett.* **86** 3435–8

[20] Deamer D W and Branton D 2002 *Acc. Chem. Res.* **35** 817–25

[21] Vercoutere W, Winters-Hilt S, Olsen H, Deamer D, Haussler D and Akeson M 2001 *Nat. Biotech.* **19** 248–52

[22] Howorka S, Movileanu L, Braha O and Bayley H 2001 *Proc. Natl Acad. Sci., USA* **98** 12996–3001

[23] Kasianowicz J J, Burden D L, Han L C, Cheley S and Bayley H 1999 *Biophys. J.* **76** 837–45

[24] Braha O, Gu L Q, Zhou L, Lu X, Cheley S and Bayley H 2000 *Nat. Biotech.* **18** 1005–7

[25] Gu L Q, Braha O, Conlan S, Cheley S and Bayley H 1999 *Nature* **398** 686–90

[26] Bayley H and Cremer P 2001 *Nature* **413** 226–30

[27] Coulter W H 1953 US Patent 2,656,508

[28] DeBlois R W and Bean C P 1970 *Rev. Sci. Instrum.* **41** 909–15

[29] Bezrukov S M, Vodyanoy I and Parsegian V A 1994 *Nature* **370** 279–81

[30] Szabò I, Bàthori G, Tombola F, Brini M, Coppola A and Zoratti M 1997 *J. Biol. Chem.* **272** 25275–82

[31] Kasianowicz J and Bezrukov S M 1995 *Biophys. J.* **69** 94–105

[32] Meller A and Branton D 2002 *Electrophoresis* **23** 2583–891

[33] Henrickson S E, Misakian M, Robertson B and Kasianowicz J J 2000 *Phys. Rev. Lett.* **85** 3057–60

[34] Bhakdi S and Tranum-Jensen J 1991 *Microbiol. Rev.* **55** 733–51

[35] Gouax J E, Braha O, Hobaugh M R, Song L, Cheley S, Shustak C and Bayley H 1994 *Proc. Natl Acad. Sci., USA* **91** 12828–31

[36] Jonas D, Walev I, Berger T, Liebetrau M, Palmer M and Bhakdi S 1994 *Infect. Immun.* **62** 1304–12

[37] Bantel H, Sinha B, Domschke W, Peters G, Schulze-Osthoff K and Jänicke R U 2001 *J. Cell Biol.* **155** 637–47

[38] Menestrina G 1986 *J. Membr. Biol.* **90** 177–90

[39] Song L, Hobaugh M R, Shustak C, Cheley S, Bayley H and Gouax J E 1996 *Science* **274** 1859–65

[40] Lubensky D K and Nelson D R 1999 *Biophys. J.* **77** 1824–38

[41] Tinland B, Pluen A, Sturm J and Weill G 1997 *Macromolecules* **30** 5763

[42] Sung W and Park P J 1996 *Phys. Rev. Lett.* **77** 783–6

[43] Muthukumar M 1999 *J. Chem. Phys.* **111** 10371–4

[44] Muthukumar M 2001 *Phys. Rev. Lett.* **86** 3188–91

[45] Eisenriegler E 1993 *Polymers Near Surfaces* (Singapore: World Scientific)

[46] Risken H 1989 *The Fokker–Planck Equation* (Berlin: Springer)

[47] Slonkina E and Kolomeisky A 2003 *J. Chem. Phys.* **118** 7112–18

[48] Chuang J, Kantor Y and Kardar M 2002 *Phys. Rev.* E **65** 011802

[49] Chern S-S, Cárdenas A E and Coalson R D 2001 *J. Chem. Phys.* **115** 7772–82

[50] Kong C Y and Muthukumar M 2002 *Electrophoresis* **23** 2697–703

[51] Loebl H C, Goodwin S P and Matthai C C 2003 *Phys. Rev.* E at press

[52] Ambjörnsson T, Apell S P, Konkoli Z, Di Marzio E A and Kasianowicz J J 2002 *J. Chem. Phys.* **117** 4063–73

[53] Doi M and Edwards S F 1986 *The Theory of Polymer Dynamics* (Oxford: Clarendon)

[54] Nakane J, Akeson M and Marziali A 2002 *Electrophoresis* **23** 2592–601

[55] Colquhoun D and Hawkes A G 1995 *Single-Channel Recording* ed B Sakmann and E Neher (New York: Plenum)

[56] Arnott S, Chandrasekaran R and Leslie A G W 1976 *J. Mol. Biol.* **106** 735–48

[57] Saenger W 1988 *Principles of Nucleic Acid Structure* (New York: Springer)

[58] Bates M, Burns M and Meller A 2003 *Biophys. J.* **84** 2366–72

[59] Bates M, Burns M and Meller A, manuscript in preparation

[60] Andersen O S 1999 *Biophys. J.* **77** 2899–901
[61] Deamer D W and Akeson M 2000 *Tibtech* **18** 147–50
[62] Marziali A and Akeson M 2001 *Annu. Rev. Biomed. Eng.* **3** 195–223
[63] Branton D 2002 private communication
[64] Li J, Stein D, McMullan C, Branton D, Aziz M J and Golovchenko J A 2001 *Nature* **412** 166–9
[65] Ling S 2002 private communication